(Project Number: 945 041)

DELIVERABLE

D2.4 Main Heat Exchanger

Lead Beneficiary: CENTRUM VYZKUMU REZ

Due date: 30/09/2023 Released on: 26/10/2023

Authors:	Petr Vácha, Tomáš Melichar, Roman Koryčanský, Daniel Kříž, Gusztáv Mayer, Zsombor Bali

For the Lead Beneficiary	Reviewed by Work package Leader	Approved by Coordinator
Tomáš MELICHAR	**Jana KALIVODOVA**	**Branislav HATALA**

Start date of project: **01/10/2020** Duration: **48 Months**
Project Coordinator: **Branislav Hatala**
Project Coordinator Organisation: **VUJE, a. s.** VERSION: 1.1

Project co-funded by the European Commission under the Euratom Research and Training Programme on Nuclear Energy within the Horizon 2020 Programme		
Dissemination Level		
PU	Public	**X**
RE	Restricted to a group specified by the Beneficiaries of the SafeG project	
CO	Confidential, only for Beneficiaries of the SafeG project	

Version control table

Version number	Date of issue	Author(s)	Brief description of changes made
1.0	26.10.2023	Tomas Melichar	1st draft
1.1	26.10.2023	Jakub Heller	Reviewed by the consortium and MST Final version

Project information

Project full title:	Safety of GFR through innovative materials, technologies and processes
Acronym:	SafeG
Funding scheme:	Research and innovation action
ECGA number:	945041
Programme and call	Horizon 2020 Framework Programme for Research and Innovation (2014-2020) NFRP-2019-2020 (Nuclear Fission and Radiation Protection Research)
Coordinator:	Dr. Branislav Hatala
EC Project Officer:	Dr. Cristina Fernandez Ramos
Start date – End date:	01/10/20 – 30/09/2024 i.e. 48 months
Coordinator contact:	+421 905 567 985, branislav.hatala@vuje.sk
Administrative contact:	+420 602 771 784, jakub.heller@evalion.cz
Online contacts (website):	www.safeg.eu

„This project has received funding from the Euratom research and training programme 2019-2020 under grant agreement No 945041".

EXECUTIVE SUMMARY

A pre-conceptual design of the main heat exchanger for the ALLEGRO reference parameters was elaborated and is described in this deliverable. The main heat exchanger makes the interface between the primary helium circuit and secondary energy conversion circuit with nitrogen and helium mixture. The design of shell&tube heat exchanger is presented in the form of 3D model and main operational parameters. The model is supported by technical calculations. Moreover, CATHARE thermal-hydraulic model of ALLEGRO was updated with the new main heat exchanger design and both steady-state and transient simulations were performed. Alternative heat exchanger design based on microchannel layout was also investigated for the ALLEGRO relevant parameters.

This document is prepared in compliance with the template provided by the Commission in Annex 1 of the Guidelines on Data Management in Horizon 2020.

LIST OF ABBREVIATIONS

CVR	Centrum výzkumu Řež
EK	Centre for Energy Research
GFR	Gas-cooled Fast Reactor
HX	Heat Exchanger
PCHX	Printed Circuit Heat Exchanger
PFHX	Plate Fin Heat Exchanger
KVK	The Component Testing Facility
MHX	Main Heat Exchanger
STH	Systemic Thermal-hydraulic
V/HTR	Very High Temperature Reactor

CONTENT

1 INTRODUCTION

A new preconceptual design of the main heat exchanger (MHX) for ALLEGRO was elaborated within SafeG project WP2 and is described in this deliverable. The MHX makes an interface between the primary helium circuit and the secondary energy conversion circuit. In this work, nitrogen and helium mixture is considered as a working fluid of the secondary circuit, based on inputs from parallel activities. In the ALLEGRO layout, two MHXs are considered, designed to 41.25 MW thermal power each. The primary helium operational parameters ae characterized by inlet / outlet helium temperature of 850 °C / 400 °C, helium pressure of 7 MPa and flow rate of 17.66 kg/s. On the secondary side, parameters of the nitrogen/helium (90/10 %) are inlet / outlet temperature of 830 °C / 380 °C, nominal pressure of 22.5 MPa and mass-flow rate of 58.5 kg/s.

In this work, a 3D model of the new shell&tube MXH was elaborated by UJV, based on previous experience from V/HTR. The model was supported by technical calculation. The description and justification of the design is presented in this deliverable. The CATHARE thermal-hydraulic model of ALLEGRO was updated with the new MHX by EK and both the steady-state and transient simulations were performed. The description of the updated model, simulations results and conclusions of this study are presented as a separate technical report attached to this deliverable (Appendix 1). An alternative HX design compatible with the ALLEGRO parameters based on microchannels layout was investigated by CVR. Moreover, design and operational experience from the large-scale experimental facility related to the MHX is also shared.

2 SELECTION OF THE HEAT EXCHANGER TYPE

There are many technologies available for transferring heat between fluid streams, for example shell and tube heat exchangers, plate heat exchangers, direct contact heat exchangers, adiabatic wheels and so on. The selection of the optimum technology for the application depends on many factors. When speaking of high-temperature gas-gas heat exchangers, there are in principle two main types to be considered as the most suitable, according to [1] or [2]

- Helical coil tube-and-shell heat exchanger
- Plate-type heat exchanger

A thorough study of the available technologies and their implications to the design, lifetime and cost of the GFR main heat exchanger was summarized in one of the previous GFR-oriented projects [3].

2.1 Helical coil heat exchangers

Helical coil heat exchangers belong to the shell and tube family of heat exchanger designs and consist of a pressure retaining outer shell and a tube bundle. One fluid passes through the outer shell and the second one passes through the tube bundle. Heat moves through the walls of the tube bundle from the hot fluid to the cold fluid. This type of heat exchanger is well understood and widely employed and a basis for construction under ASME III exists.

Shell and tube heat exchanges are typically categorised according to the configuration of the tube bundle and shell. For the purpose of this report, we will distinguish between —conventional shell and tube heat exchangers and shell and tube heat exchangers where the tube bundle is helical. All previous high temperature gas reactors have employed helical tube bundle heat exchangers as with this tube configuration the fluid flow over the bundle approaches the ideal cross flow. This allows a smaller heat exchanger to be used for a given duty compared to straight or U-tube design. A helical coil tube bundle is illustrated in Figure 2-1.

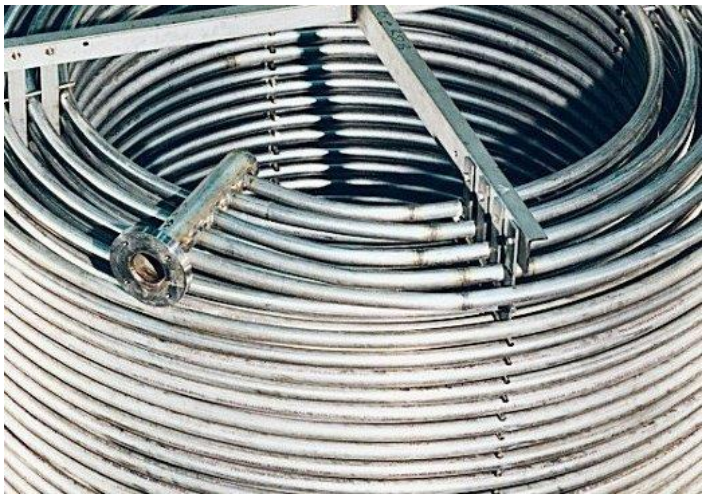

Figure 2-1: Helical coild tube bundle [https://www.graham-hart.com/products_coil_heat_exchangers.php]

A large design and testing programme took place in Germany during the 1970's and 1980's, including long-term and large-scale demonstration experiments. The Component Testing Facility (KVK) was used for the experimental testing of high-temperature components for nuclear coal gasification. Its main parameters are listed in Tab. 2-1.

Tab. 2-1: The KVK test facility parameters

Parameter	Value	Unit
Thermal power	10	MW
Primary inlet/outlet Temperature	950 / 290	°C
Secondary inlet/outlet Temperature	220 / 900	°C
System pressure	40	bar
Nominal mass flow rate	3	kg/s
Helium velocity	Up to 60	m/s
Temperature transients rate	200	K/min
Pressure transient rate	5	bar/s

As can be seen from Tab. 2-1, the parameters of the test facility were in the same order as the design values of ALLEGRO, hence the results are of high importance for the design of the MHX of ALLEGRO.

From the summary of the post-test examinations [4], it can be seen, that:

- The helium tightness of the overall facility is good. It amounts to < 1 kg/d.
- He-blowers, steam generator and steam-heated helium preheater operated reliably.
- The selected materials for internal insulations proved themselves right away.
- The components did not show any inadmissible vibrations.
- The required helium atmosphere can be easily adjusted using the available helium purification and dosing system.
- The surfaces of materials in the high-temperature zone between 900° C and 950° C exhibit a stable chromium oxide protective coating. This is also valid for the included metal samples, which can be exchanged during operation.
- Until to the end of the testing phase of KVK, it has been possible to convert and extend the KVK without any problems and within a short time.

These results, complemented by the fact, that these kinds of heat-exchangers are easily maintained and inspected during outages, show that the design of ALLEGRO MHX using the helical coil technology made from nickel-based alloys is viable a should be considered as the reference option for the moment.

2.2 S-Allegro MHX

It is worth to mention that there is also a special design of the helical coil based heat exchanger implemented in the S-Allegro facility. This primary HX is located between the primary and secondary helium circuit. The nominal thermal power is 1 MW.

The primary HX is the biggest component of the facility. The diameter is approx. 1.5 m and height is approx. 5 m. The large dimensions of the heat transfer area are given by relatively high convective heat transfer resistance at both sides (gas-gas HX). The primary helium flows in the tube side, secondary helium in the shell side. The primary (hot) helium enters from the bottom through the inner leg of the coaxial pipe and flows through the tube sheet on the tube side. The tube side is made of 268 helical tubes. The coil length is 2.3 m, each tube has 4.895 m. In the top part, the tubes turn 180° and are guided downwards through the outer annular volume. The heat transfer and pressure loss in this part is low as the tubes are straight and low velocity flow is reached in the shell side. Helium exits the component through the outer leg of the coaxial pipe. The secondary (cold) helium enters the shell side through the outer leg of the secondary

pipe. It flows downwards through the outer downcomer and then turns 180° and flows upwards through the upcomer. Secondary helium leaves the PHX through the central upcomer (5) into the inner leg of the secondary pipe. The primary HX of the S-Allegro facility during transport to the facility site is shown in Figure 2-1. The primary HX installed in the S-Allegro facility is then shown in Figure 2-3. The heat exchanger as well as whole the loop was designed and delivered by ATEKO a.s. company.

Figure 2-2: Primary heat exchanger of S-Allegro facility (transportation)

Figure 2-3: Primary heat exchanger of S-Allegro facility (installed)

Although the S-Allegro facility has not been operated at the maximum power level yet, various experimental campaigns were carried out at different power and temperature levels. No design issues related to the primary HX were observed. It can be concluded, based on operational experience, that the component is designed properly. Selected experimental data including inlet and outlet temperatures, pressure levels and mass-flow rates are presented in the SafeG project deliverable 5.3 within the STH benchmark [5].

2.3 Microchannel plate-type heat exchangers

Plate-type heat exchangers might be an alternative option, not only for the main HX but for basically all heat transfer components. An attention might be paid specifically on the microchannel HXs that have potential for compact solution (low dimensions) and applicability for high operational parameters. The potential of microchannels HXs grows with increasing abilities of advanced manufacturing processes such as diffusion welding or 3D printing. The microchannels HXs are being implemented within various industrial processes and relatively high number of suppliers can deliver such components. The MW-scale microchannel HX are commercially available for temperatures around 500 °C a pressure above 20 MPa. However, availability of such components compatible with extreme parameters assumed in the ALLEGRO main HX is still limited and requires further development and testing.

The printed-circuit HX (PCHX) is based on plates with etched channels that are connected using diffusion welding. The dimension of the channels can be lower than 1 mm. A basic scheme of the PCHX is shown in Figure 2-4.

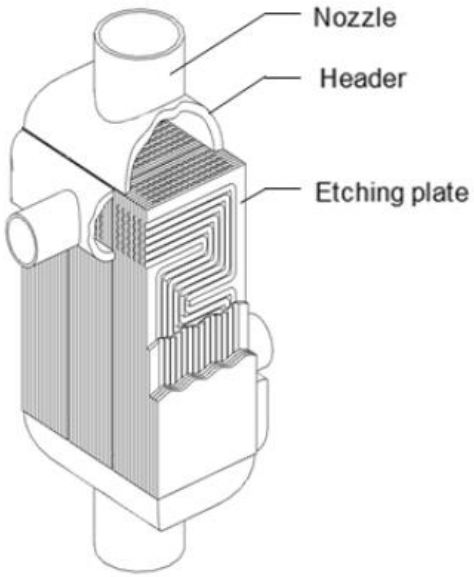

Figure 2-4: An example of PCHX (https://www.kobelco-machinery-energy.com/en/energy/heat-exchanger/dche/)

The channels and heat transfer area in plate-fin HXs (PFHX) is made of plates bent in small waves. This allows to make different shape / cross-section between the cold and hot side. An example of the PFHX is shown in Figure 2-5.

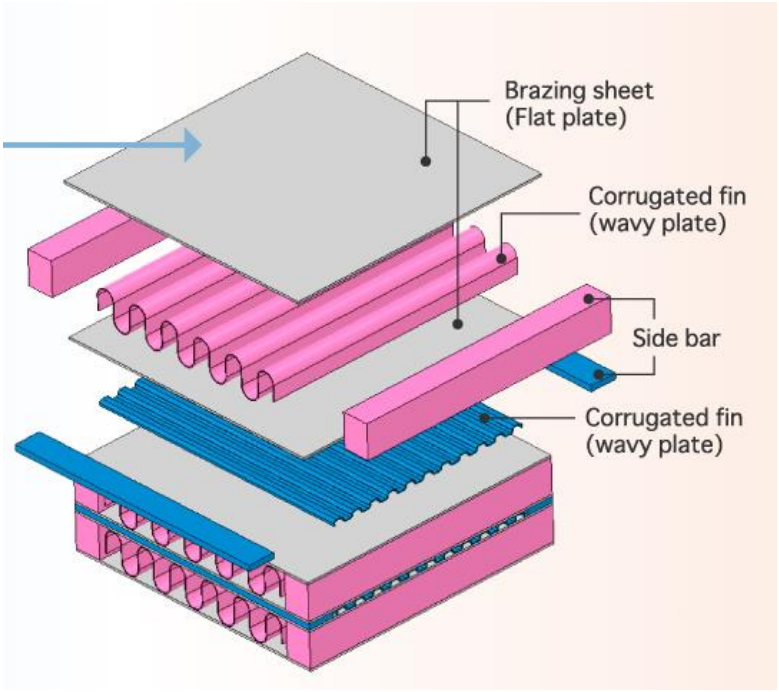

Figure 2-5: An example of PFHX (https://www.spp.co.jp/netsu/en/products/smalex/)

Due to limited availability of microchannel HXs in the relevant scale for the ALLEGRO parameters, this type of HXs is considered as an alternative option in this report. A computational model of PCXH was prepared to provide comparison with the shell&tube HX (see section 4).

3 DESIGN OF THE ALLEGRO MHX

The design process of the heat exchanger has begun with assessing its target applications, and the main fixed parameters. The high-level target is to allow ALLEGRO to reach high temperatures of its secondary coolant, and, therefore, to allow for successful demonstration of GFR capabilities in cogeneration and hydrogen production. The secondary objective is to get rid of water in the secondary system, which could, in case of an unmitigated leak, comprise the safety of ALLEGRO as it is a fast reactor sensitive to presence of a substantial amount of moderator in the core.

There is another level of complexity in the designing process of the MHX of ALLEGRO, because of the two-step strategy in its operation. First, the so-called "driver core" will be loaded, with the core inlet/outlet temperature of 260/530 °C. It will be then replaced by the "refractory core" with 400/850 °C, and also lower total mass flow rate. It is not physically possible to fully optimize the main heat exchanger for both the configurations due to the different temperature levels, temperature gradients, and mass flow rates. Replacing the MHX after several years under operation would also present a major task connected with substantial economic and technical challenges.

Since the goal of the MHX is to allow showcase of the possibilities of GFR, it was decided that the full optimization will be done for the high-temperature refractory core, and the final design of the MHX will be just checked against the driver core values if it is capable to dissipate enough heat. Tab. 3-1 summarizes the fixed input data for the design process:

Tab. 3-1: Fixed parameters of the MHX

Parameter	Value	Unit	Note
Required heat transfer	41.25	MW	Nominal power/2 · 1.1
HX inlet temperature	850	°C	
HX outlet temperature	400	°C	
Primary pressure	7	MPa	Nominal primary pressure
Target height of the active part of the MHX	2.0	m	To fit inside the current version of guard vessel
Central channel diameter	0.762	m	To allow smooth transition from the primary duct
Central channel thickness	20	mm	To comply with RCC-MRx code
Coil tube inner diameter	16	mm	To comply with RCC-MRx code
Coild tube thickness	2	mm	To comply with RCC-MRx code

In addition to the parameters listed in Tab. 3-1, there are other requirements entering the design process. In order to achieve high reliability and safety of the MHX, the design must allow for in-service inspections and easy repair of leaking tubes. In order to ensure sufficient capacity for heat transfer throughout the lifetime of the reactor, the design required heat transfer is 55 % of the nominal power for each of the two main heat exchangers, resulting in total of 110 % design power. In order for the HX to work effectively and allow showcase of GFR capabilities in high-temperature applications, the target approach temperature is maximum 20 °C.

3.1 Deriving the main MHX parameters

For easily adjusting the design, a simple script using MS Excel was created, that derives the geometry and main calculated parameters from the fixed parameters, and by using the open database of material properties available at nist.gov [6]. Using this script, following values were obtained for the primary and the secondary sides of the HX.

Primary side of the HX

T1	*850 °C*
T2	*400 °C*
T_{avr}	*625 °C*
P	*7 MPa*
ρ_{pr}	*4,27 kg/m3*
η	*4,29 E-05 kg/m*s*
ν	*1 E-05 m2/s*
λ	*0,337 W/m*K*
cp	*5189,5 J/kg*K*
Pr	*0,6607*

Mass flow rate:

$$\dot{m} = \frac{Q}{cp*(T1-T2)}$$

$$\dot{m} = 17{,}66\ \mathrm{kg/s}$$

Coil tubes parameters:
Since pipes are coiled at pitch angle 10° their projection into primary side flow channel is an ellipse.

$$d_{el} = d_2 \sin(\beta)$$

$$o_{el} = \frac{\pi}{4} * \sqrt{2 * \left({d_2}^2 - {d_{el}}^2\right)}$$

$$o_{el} = 0{,}236\ m$$

$$s_{el} = \frac{\pi}{4} * d_2 * d_{el}$$

Primary side flow channel forms a ring between central channel and outside shell, filled by coil of pipes. Pipes are coiled in multiple rings around central channel, spacing between rings and channel walls is set to 0,015 m between wall and ring and 0,025 m between rings. Number of rings and by extension diameter of outside shell, is result of iterative computation.

l1	*0,015 m*
l2	*0,025 m*
n	*number of rings*

Outer shell inner diameter:

$$D_3 = D_2 + 2 * l_1 + (n-1) * l_2$$

Primary side flow channel:

n_{tr}	*number of pipes in channel*

number of pipes is given by Tab. 3-2, numbers are set to keep spacing between pipes in ring in range 0.0052 m to 0.0061 m.

Tab. 3-2: Number of pipes in individual rings

ring	n. pipes
1	18
2	19
3	20
4	21
5	22
6	23
7	24
8	25
9	26
10	27
11	28
12	29
13	30
14	32
15	33

$$S_{prim} = \frac{\pi * {D_2}^2}{4} - \frac{\pi * {D_3}^2}{4} - n_{tr} * s_{el}$$
$$S_{prim} = 0{,}656\ m^2$$

Flow speed:

$$u_{pr} = \frac{\dot{m}}{S_{prim} * \rho_{pr}}$$
$$u_{pr} = 6{,}3\ m/s$$

Hydraulic diameter on the primary side:

$$d_h = \frac{S_{prim}}{o}$$

$$d_h = \frac{S_{prim}}{\pi * D_1 + \pi * D_3 + n_{tr} * o_{el}}$$
$$d_h = 0{,}0272\ m$$

Reynolds number:

$$Re = \frac{u_{pr} * d_h}{\nu}$$
$$Re = 17093$$

Nusselt number:

Formula taken from [6]

f_a $0{,}927$

$$Nu = 0{,}1286(fa * Re)^{0{,}692} * Pr^{\frac{1}{3}}$$
$$Nu = 90{,}276$$

Thermal diffusivity:

$$\alpha_{pr} = \frac{Nu * \lambda}{d_h}$$
$$\alpha_{pr} = 1091\ W/m * K$$

Secondary side of the HX

Again, all the material properties data were taken from [7].

T1	*830 °C*
T2	*380 °C*
T_{avr}	*605 °C*
P	*22,5 MPa*
ρ_{pr}	*72,67 kg/m3*
η	*3,96 E-05 kg/m*s*
ν	*5,44 E-07 m2/s*
λ	*0,0904 W/m*K*
cp	*1567,21 J/kg*K*
Pr	*0,686*

Mass flow

$$\dot{m} = \frac{Q}{cp*(T1-T2)}$$
$$\dot{m} = 58{,}49 \text{ kg/s}$$

Flow speed

$$S_{sec} = \frac{\pi*d_1}{4} * n_{tr}$$
$$u_{sec} = \frac{\dot{m}}{S_{sec}*\rho_{pr}}$$
$$u_{sec} = 10{,}61\ m/s$$

Hydraulic diameter

$$d_h = d_1$$

Reynolds number

$$Re = \frac{u_{pr}*d_h}{\nu}$$
$$Re = 311791{,}42$$

Nusselt number

on secondary side, formula for flow inside a pipe is used:

$$Nu = 0{,}024 * Re^{0,8} * Pr^{0,25}$$
$$Nu = 542{,}57$$

Thermal diffusivity

$$\alpha_{sec} = \frac{Nu*\lambda}{d_h}$$
$$\alpha_{sec} = 3065{,}54\ W/m*K$$

Pipe material heat conductivity

λ_{tr}=20 W/mK

Logarithmic mean temperature difference

$$\Delta T_{ln} = \frac{\Delta T_{in}-\Delta T_{ut}}{ln\frac{\Delta T_{in}}{\Delta T_{out}}}$$
$$\Delta T_{ln} = 20\ K$$

Heat transfer coefficient for pipe:

$$k = \frac{2 * \pi}{\frac{1}{\alpha_{prim}} + \frac{1}{\lambda} ln \frac{d_2}{d_1} + \frac{1}{\alpha_{sek}}}$$
$$k = 507\ W/mK$$

Required length of pipe:

$$l = \frac{Q}{k * \Delta T_{ln}}$$
$$l = 4063{,}42\ m$$

Required number of pipes:

Length of single pipe based on pipe pitch and exchanger height.

$$l_{tr} = \frac{h}{sin\beta}$$
$$l_{tr} = 11{,}52m$$

Required number of pipes:

$$n_{tr=\left|\frac{l}{l_p}\right|}$$
$$n_{tr} = 353$$

Based on data in Tab. 3-2, 15 rings of coil tubes are required to get at least 353 pipes, with the actual number of pipes in the 15 rings is 377, which gives another 6.7 % margin above the calculated amount.

3.2 Summary of main parameters of the MXH

The final conceptual design of the main heat exchanger is a gas-to-gas helical coil tube-and-shell heat exchanger, with the primary helium gas flowing on the shell side, and a 90 % nitrogen 10 % helium mixture on secondary side flowing inside the tubes.

Both the primary and the secondary main ducts use coaxial ducts, where the cold side flow in the outer channel, so the pressure-stressed outside wall is exposed to lower temperatures. The main blower is mounted on the bottom of the heat exchanger vessel, and is of radial type.

Main operation parameters are summarized in Tab. 3-3.

Tab. 3-3: Summary of MHX parameters

Parameter	Primary side	Secondary side
Total power	41.25 MW	41.25 MW
Inlet temperature	850 °C	380 °C
Outlet temperature	400 °C	830 °C
Mass flow rate	17.66 kg/s	58.5 kg/s
Coolant pressure	7 MPa	22.5 MPa
Flow velocity	6.30 m/s	10.61 m/s
Flow area	0.656 m2	0.076 m2
Nr. of helical coil tubes	377	
Helical tubes inclination	10°	
Helical tubes length	11.5 m	
Material of the helical coil tubes	Inconel 617	

3.3 CAD design of the MHX

All the above-mentioned calculated design parameters were transferred to a 3D CAD model, which will be put into to reference CAD model of ALLEGRO. Following is a general overview of the design.

The flow pattern for both sides of exchanger is highlighted in Figure 3-1. The secondary gas (blue) come through outer tube which transitions into vertical tube in the middle of the exchanger at the end of which is the lower plenum. From this plenum, the secondary gas enters into the helical tubes leading to the upper plenum, from where it goes to the inner tube.

The primary gas enters the inner vessel and continues down along the helical tubes on the shell side, into the main blower. The blower outlet leads into the outside pressure vessel, from where the coolant continues further into the outer primary tube.

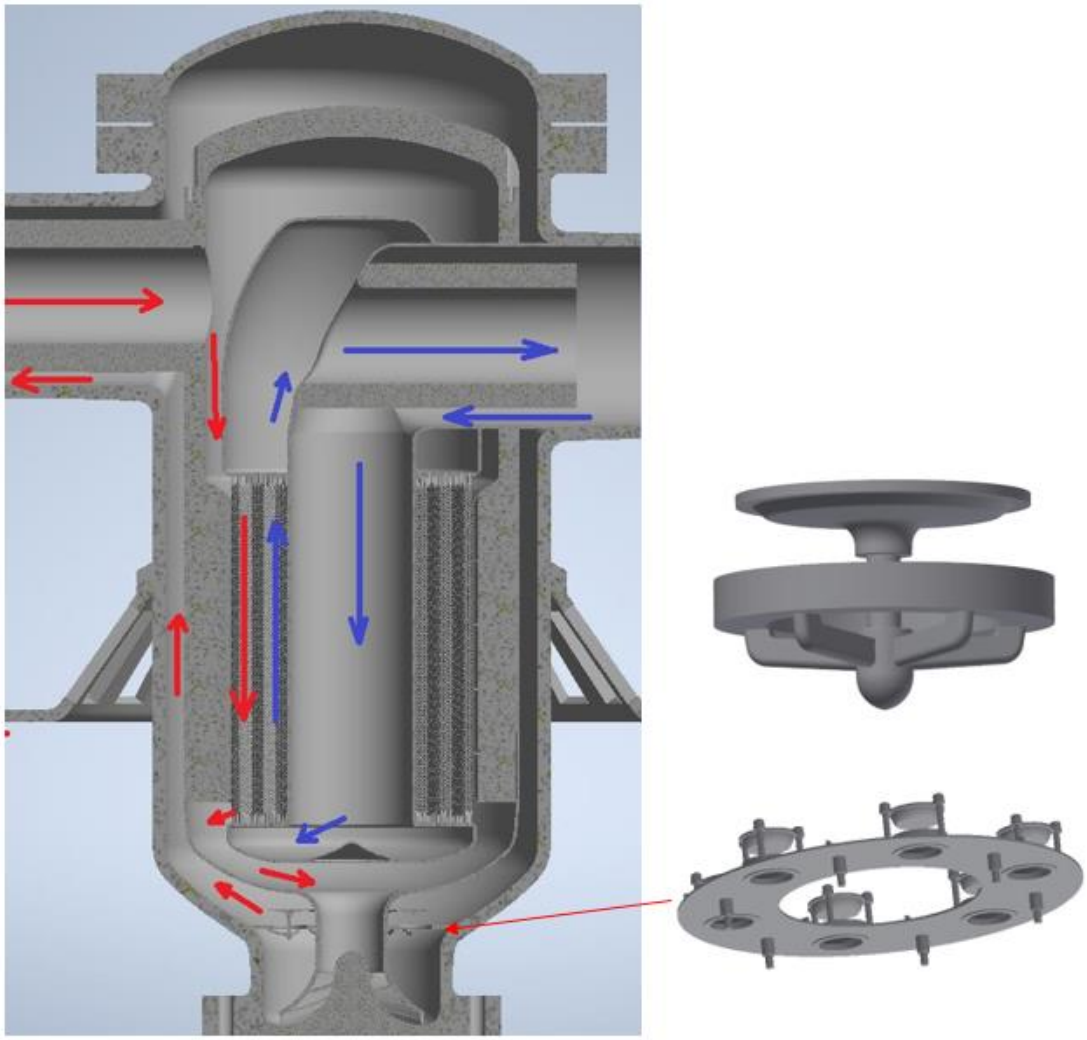

Figure 3-1: Primary (red) and secondary (blue) flow patterns inside the main heat exchangers

The hot gas inside the inner vessel is insulated from the cold gas in the outer vessel, the layer of insulation is visible in Figure 3-2, as well as the primary and the secondary ducts, and the helical tubes. The helical coil tubes are arranged in 14 rings coiled around the central tube. A section showing several of the tubes in the outermost ring is shown in Figure 3-3. The direction

in which the tubes are wrapped changes from clockwise to anticlockwise each three layers, to enhance the turbulence of the flow.

Main heat exchanger is designed to work in forced convection, in case loss of power either due to transient or intentional shutdown, the cooling is overtaken by the DHR exchangers. For their proper function, it is necessary to disconnect the main heat exchanger. For this purpose, a set of isolation valves are placed at the blower output. The valves work passively, being lifted by the pressure generated by the main blower, and after it stops, they slide down and close the flow path. Their design is shown in Figure 3-1.

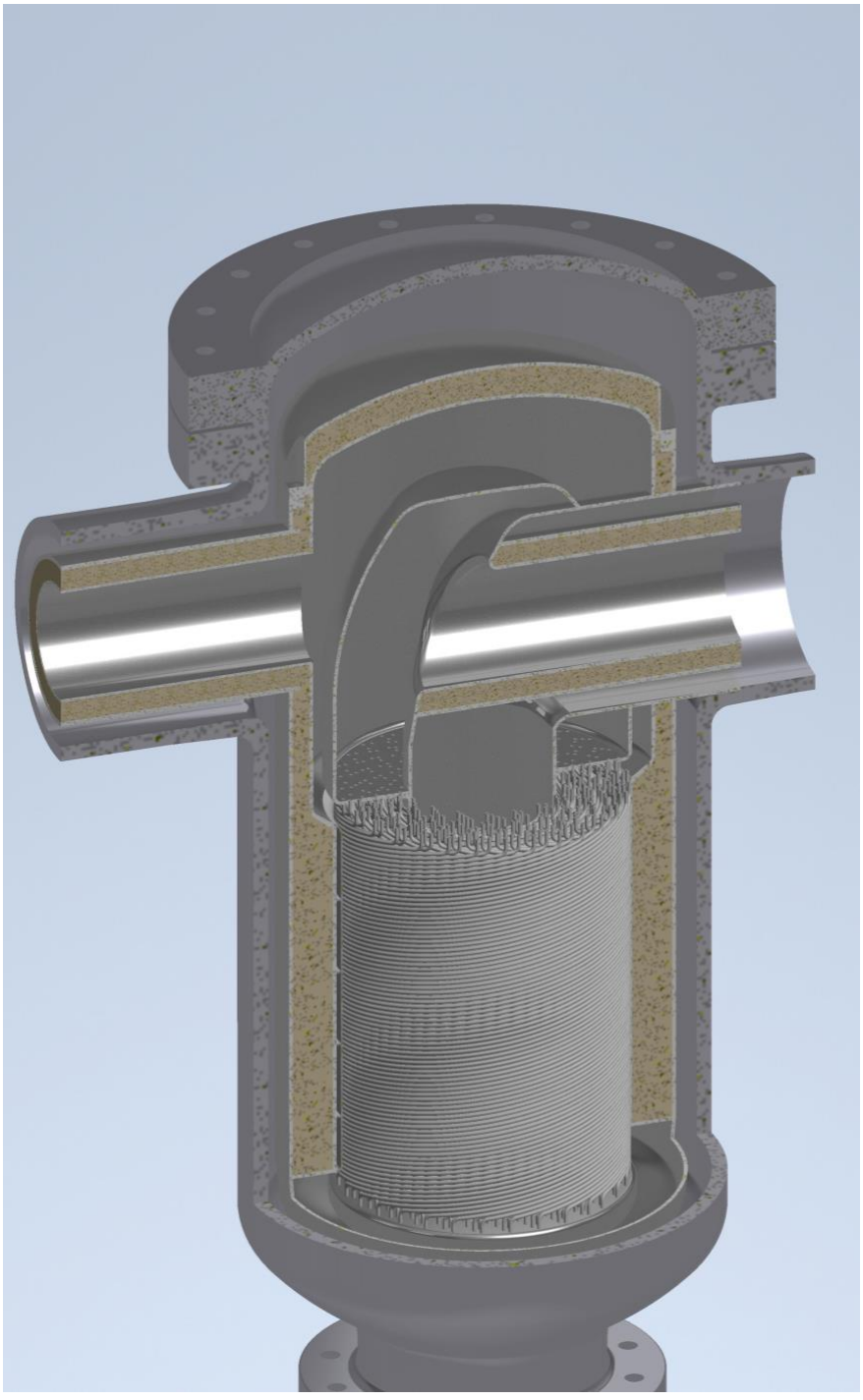

Figure 3-2: MXH cross-section view

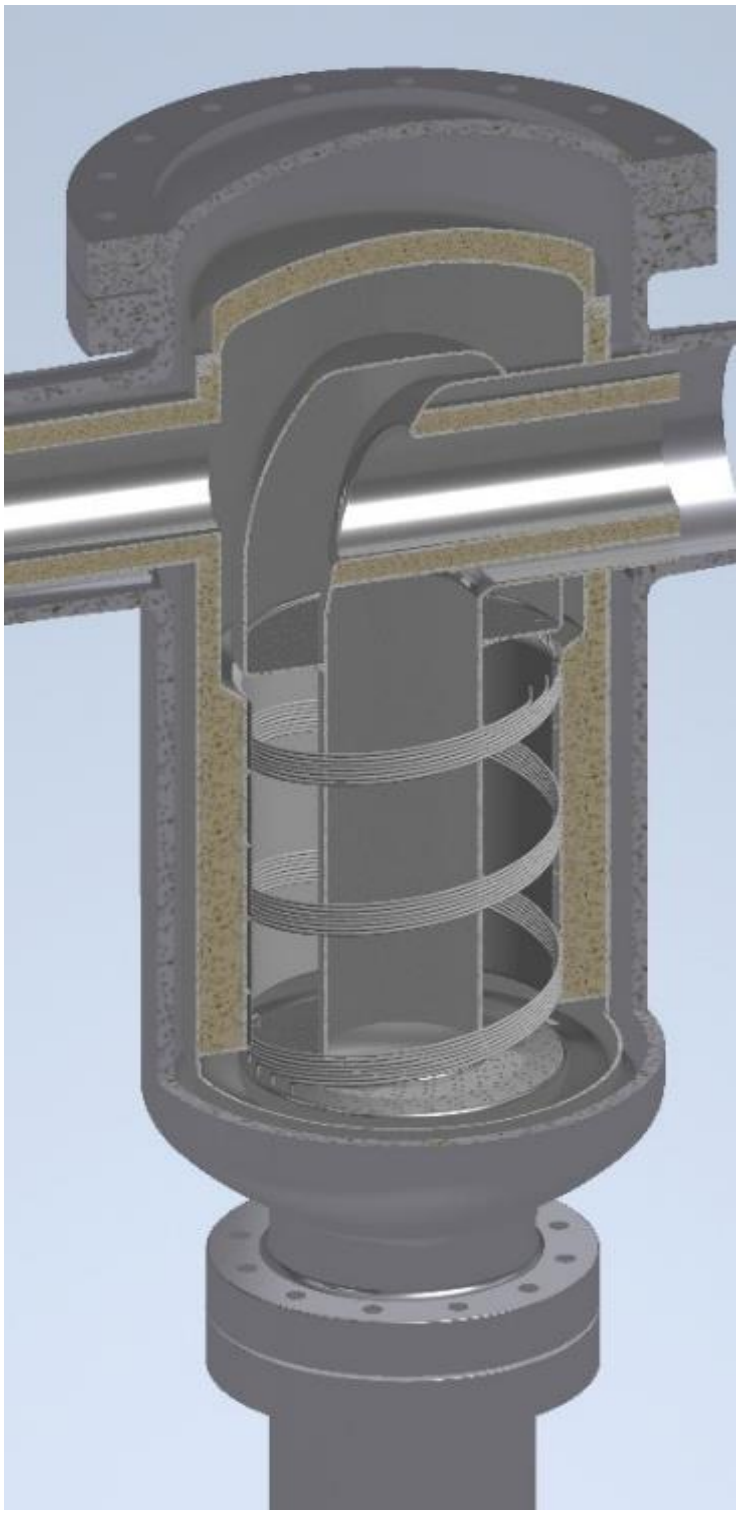

Figure 3-3: Outer layer of helical tubes

4 PROPOSAL OF PCHX

A preliminary thermal and geometric proposal of PCHX compatible with the ALLEGRO MXH parameters was elaborated as an alternative option to the shell&tube HX. The geometric proposal is based on a numerical model prepared using Modelica Dymola software. The geometric parameters were optimized to fit the required inlet and outlet temperatures and flow rates and to reach reasonable pressure loss (approx. 1 bar). The resulting proposal is characterized by the external dimensions of 3.72 × 1.25 × 0.96 m. The number of channels is 150 000, width of a channel is 2 mm. The summary of the main geometric and thermal-hydraulic parameters is given in Tab. 4-1. Selected dimensions are indicated in Figure 4-1.

Tab. 4-1: Main geometric and thermal-hydraulic parameters of the PCHX-based main HX

Geometric parameters				
Heat transfer area	*Ah*	m^2	2869	
Channels no.	*N*		150000	
Total length	*L*	*m*	3.72	
Total width	*W*	*m*	1.25	
Total hight	*H*	*m*	0.96	
Thermal-hydraulic parameters				
			Primary	Secondary
Avg. flow velocity	*v*	*m/s*	18.9	4.6
Avg. Re	*Re*		2150	7276
Avg. heat transfer coefficient	*α*	W/m^2K	1766	1579
Avg. Heat transport coefficient	*k*	W/m^2K	770	
Lomaritmic mean temperature difference	*LMTD*	*K*	18.67	
Power	*Q*	*MW*	41.26	
Inlet temperature	*Tin*	*°C*	850	380
Outlet temperature	*Tout*	*°C*	400	830
Flow rate	*m*	*Kg/s*	17.66	58.5
Pressure level	*p*	*MPa*	7	22.5
Pressure loss	*dp*	*bar*	1.10	0.60

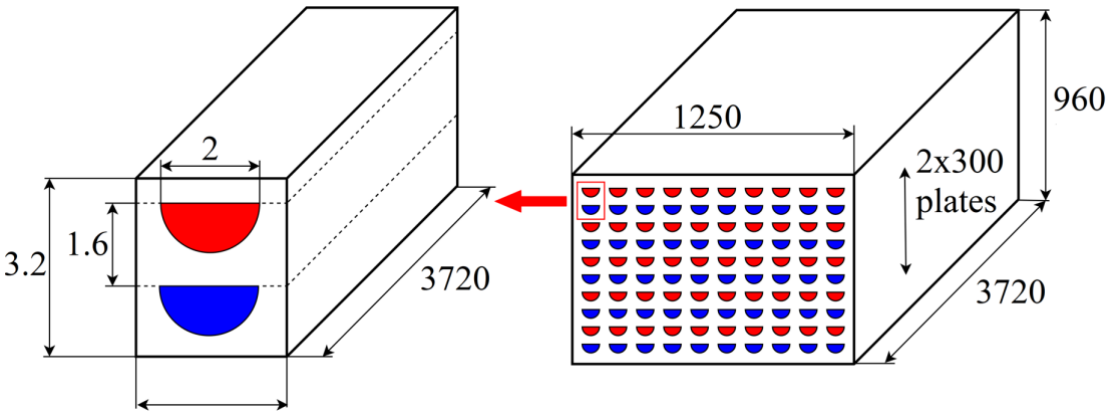

Figure 4-1: Main dimension of the PCHX-based main HX

5 CONCLUSION

This document describes a preconceptual design of the main HX compatible with the ALLEGRO parameters. The HX design is based on shell&tube type and experience from the HTR. The 3D CAD model supported with technical calculations was elaborated. The outcome of this work will be used as a new input for the ALLEGRO design database. The new main HX design was also implemented in the thermal-hydraulic CATHARE model of ALLEGRO and several steady-states and transient cases were simulated. The results of these simulations as well as the model are described in Appendix 1 of this report.

Apart from this, an alternative option of the main HX based on an innovative printed-circuit HX type was investigated. Although the availability of such component in a relevant scale and compatible with the ALLEGRO parameters is still limited, the basic geometric and thermal-hydraulic proposal was carried out and fits to the required parameters. This type of HX might increase the flexibility of the system due to the compact solution and low dimension so it is worth observing progress in the innovative HX R&D within the further stages of the GFR/ALLEGRO development.

6 REFERENCE

[1] General Atomics. NGNP IHX and Secondary Heat Transport Loop Alternative Study. 2008. 911119 Revision 0.

[2] Wheatley, W. Intermediate Heat Exchanger Design Options for the High Temperature Gas Reactor. s.l. : University of Manchester, 2009. MSc Dissertation.

[3] GOFASTR: Deliverable 1-1-09 GFR Heat Exchanger Technology Report.

[4] IAEA report: https://inis.iaea.org/collection/NCLCollectionStore/_Public/21/068/21068269.pdf.

[5] T. Melichar, J. Šefl a D. Kříž, Definition of the Thermal-Hydraulic Benchmark, SafeG project deliverable, 2023.

[6] [NIST] https://webbook.nist.gov/chemistry.

[7] Esch, M., Hurtado, A., Knoche, D., & Tietsch, W. (2012). Analysis of the influence of different heat transfer correlations for HTR helical coil tube bundle steam generators with the system code TRACE. Nuclear Engineering and Design, 251, 374–380. doi:10.1.

7 APPENDIX 1 – TESTING OF THE NEW ALLEGRO MHX WITH THE CATHARE CODE

CENTRE FOR ENERGY RESEARCH

Centre for Energy Research

SafeG

EK contribution - SafeG D2.4 – Testing of the new ALLEGRO MHX with the CATHARE code

Gusztáv Mayer, Zsombor Bali

Prepared based on contract GRANT AGREEMENT NUMBER 945041 – SafeG
between the European Atomic Energy Community and Centre for Energy Research

Budapest, 2023

Address: 29-33 Konkoly-Thege Miklós rd., Budapest, H-1121
Mailing address: P.O.B.: 49, Budapest, H-1525.
E-mail: info@ek-cer.hu
Phone.: +36 1 392 2222
Webpage: www.ek-cer.hu

CONTENT

1 INTRODUCTION

When a gas-cooled reactor - like ALLEGRO - is using a steam turbine cycle to generate electricity, there is a chance that the water from the secondary circuit might leak into the primary circuit, which is called water-ingress. It could cause a positive reactivity introduction and the corrosion of the elements in the primary circuit [1]. Because of said effects, water ingress is recognised as a severe accident requiring attention.

To avoid water ingress into the core, we replaced the secondary water coolant with gas in this study. As a result, a closed Brayton cycle is used to generate electricity in the secondary circuit.

EK has contributed to investigating UJV's new gas secondary circuit by developing a model using the French CATHARE system code and providing steady state and transient results. The investigation consists of several steps.

During the SafeG input deck development in WP1, a new ALLEGRO CATHARE input deck was elaborated, which uses a 75MWth refractory core with a FUELPLAQ PWR option (This input is described in detail in SafeG D1.6). This input, which we call "WP1 REFRACTORY", has a steady state at which the core coolant inlet and outlet temperatures are 400/800 °C, respectively. Its secondary circuit contains pressurised water at 65 bar. In this work, this input deck was our primary starting point.

As a first step, using this previously mentioned CATHARE input from WP1, we elaborated a newer input with helium working fluid on the secondary side. We called this new input a "base model" throughout the text. This new input requires a secondary circuit design containing the detailed MHX, gas turbine and compressor description. Nevertheless, the detailed data are not fully ready for the gas secondary option at this state of the ALLEGRO design. Although the preliminary design of the MHX is available, the turbine and blower maps are still missing. For this reason, some assumptions had to be made concerning the turbomachinery. EK has a CATHARE input deck from previous EU projects "coupled ALLEGRO CEA" design. We used the secondary circuit of this "coupled ALLEGRO CEA" design to develop this first step. As a result, a new input was developed using the "WP1 REFRACTORY" and the "coupled ALLEGRO CEA" inputs. The secondary circuit contains helium coolant in this model, but unlike the coupled ALLEGRO CEA input, the main blower in the primary circuit is detached from the secondary shaft. The shaft in the secondary circuit connects the compressor and the turbine to the electrical grid, which means that their rotational speed is imposed in normal operation.

The next step of the current work was to replace the base model's helium coolant with a nitrogen and helium mixture and to implement the new MHX geometry. This model is called a "new model" in this chapter.

2 BASE MODEL

Several CATHARE input models were developed for the ALLEGRO reactor in the past. In this study, we started from the model developed in the SafeG project and described in SafeG D1.6. That model has a refractory core, water secondary coolant, and 400/800 C core inlet and outlet temperature. It uses the FUELPLAQ PWR option.

As a first step, we replaced the secondary water coolant with helium. This helium-cooled secondary side is called the "base" model throughout his paper. In this "base" model, the primary circuit remained untouched, but in the secondary circuit, there were some prominent changes in components.

Secondary fluid:

The secondary coolant in this base model was pure helium, so the primary and the secondary fluid were the same [2].

Turbine and compressor:

The water pump had to be replaced with a compressor, which was taken from the coupled ALLEGRO input deck [2]. A turbine had to be installed alongside the compressor to generate electricity and drive the compressor. The turbine's geometry and characteristics are the same as in the coupled ALLEGRO input deck. A shaft connected the compressor and the turbine with a generator attached to it, so the whole machine group had its rotational speed bounded by the electrical network's frequency, hence the generator's rotational speed.

Pressuriser:

In the water-filled secondary circuit used in the previous model, there was a pressuriser to control the secondary pressure and to provide a reserve for secondary coolant in case of a secondary break. This component has been removed with the introduction of the helium-filled secondary circuit.

Main heat exchanger:

The main heat exchanger's primary side remained the same, but the heat exchange area had to be reduced to stick to the 400°C core inlet temperature and the 800°C core outlet temperature. The solution was to plug some secondary tubes. Initially, there were 347 secondary tubes, which had to be reduced to 272.

With the several changes described above, an excellent steady-state could be reached with the following most important values:

Primary circuit:

- core power: 75 MW
- primary mass flow rate in one loop: 18,05 kg/s
- core inlet temperature: 400,5°C
- core outlet temperature: 800°C
- core inlet pressure: 69,72 bar
- pressure drop on the core: 0,46 bar

Secondary circuit:

- MHX power: 37,5 MW
- secondary mass flow rate in one loop: 19,45 kg/s
- MHX inlet temperature: 110,2°C
- turbine inlet temperature: 482,77°C
- turbine outlet temperature: 422,77°C
- MHX inlet pressure: 65,26 bar
- turbine inlet pressure: 62,16 bar

- turbine outlet pressure: 49,1 bar

Tertiary circuit:

- tertiary mass flow rate: 600 kg/s
- aero inlet temperature: 25°C
- aero outlet temperature: 83,25°C
- aero inlet and outlet pressure: 1 bar

3 NEW MODEL

The modifications made to the base model targeted the application of a new main heat exchanger design which has been developed by UJV. They designed a new gas-gas helical shell-and-tube type of heat exchanger. The primary and the secondary coolant enter the heat exchanger in a coaxial duct. The primary fluid flows on the shell side, and the secondary fluid flows on the tube side. The main blower is attached to the bottom of the heat exchanger.

The primary fluid, pure helium, enters the heat exchanger in the inner part of the primary coaxial duct. It is then turned downward towards the active part of the MHX. After flowing through the active part, the helium reaches the main blower, which turns it around and pumps it back up into the outer part of the coaxial duct through the outer shell of the MHX.

The secondary fluid has been changed to a mixture of nitrogen and helium. UJV used a composition of 90% nitrogen and 10% helium, which are molar percentages. A bigger amount of nitrogen is used because it has better properties for the turbomachinery. The secondary mixture enters the main heat exchanger in the outer part of the secondary coaxial duct. It flows down in the central column before turning into the helical tube bundle. As the mixture flows through the active part, it is heated up before exiting the heat exchanger in the inner part of the secondary duct.

3.1 Main heat exchanger geometry

3.1.1 Primary side

CATHARE is a one-dimensional thermal hydraulics system code, so modelling a three-dimensional geometry requires some simplifications. On the primary side, the active part of the main heat exchanger has been modelled with an axial element with a downward flow direction. In Figure EK_1 it is represented by MHX1_PRI axial element. The axial element's geometric properties are in accordance with the data provided by UJV.

In CATHARE, it is advised to connect axial elements with volume type 0 dimensional elements. Hence, a volume element contains the main isolation valve after the active part. There have been no changes made here compared to the base model.

After the main isolation valve comes the main blower following the flow. The main blower is located in the middle of an axial element (AXCIRC1 in Figure EK_1). The axial element and the blower remained unchanged.

Following another volume element, there is the outer shell of the heat exchanger modelled with an axial element with an upward flow direction. Once again, the geometrical parameters are given according to the data provided by UJV. There is no heat exchange defined on this element (ENVELOP).

Exiting the heat exchanger comes the main coaxial duct, which remained unchanged too.

3.1.2 Secondary side

On the secondary side, the first element of the heat exchanger is the central column. It is modelled with a vertical axial element with a downward flow direction (MHX1_S_C). There is no heat exchange defined on this element either, just like on the outer shell on the primary side.

After another volume element comes the active part of the heat exchanger regarding the secondary side, the tube bundle. The bundle consists of 344 helical tubes with an average inclination of 10°. It is modelled with a single axial element with the same inclination (MHX1_S_H). The average tube length is used to define the axial element's length. To be able to define heat exchange between the active part of the primary side and the active part of the secondary side, they had to have the same number of nodes. The flow area and the heated perimeter had to be defined to represent the whole tube bundle, so the values were calculated for a single tube and then multiplied by the number of tubes.

The secondary fluid enters the main heat exchanger from the compressor and leaves it towards the turbine.

Figure EK_1 shows the nodalization of the main heat exchanger and other connecting elements. The heat exchange surfaces are highlighted with light green on the edge of the corresponding axial elements. Table EK_1 explains the abbreviations seen in Figure EK_1.

Table EK_1 Abbreviations used during the modelling

Abbreviation	Meaning
HOTDUCT	The inner part of the coaxial duct in the primary circuit
HOTHX1	A volume element connecting the hot duct and the primary side of the main heat exchanger
MHX1_PRI	The primary side of the main heat exchanger's active part
VHX1CIRC	A volume element leading to the main blower's axial element
AXCIRC1	An axial element which the main blower is placed in
VCIRC1IN	A volume element connecting the main blower's axial element and the outer, inactive part of the main heat exchanger's primary side
ENVELOP	The inactive part of the main heat exchanger's primary side
ENVCOLD	A volume element leading to the cold duct
COLDUCT	The outer part of the coaxial duct in the primary circuit
MHX1_S_H	An axial element representing the helical tube bundle which is the active part of the main heat exchanger's secondary side
VHU	A volume element connecting the helical tube bundle and the axial element of the turbine
AXTURB1	An axial element where the turbine is put
MHXBY1	A bypass duct connecting the outlet of the compressor with the outlet of the turbine
AXCOMP1	An axial element which the compressor is put in
VCD	A volume element connecting the axial element of the compressor and the inactive part of the main heat exchanger's secondary side
MHX1_S_C	The inactive part of the main heat exchanger's secondary side
VMHX1	A volume element connecting the inactive and the active part of the main heat exchanger's secondary side

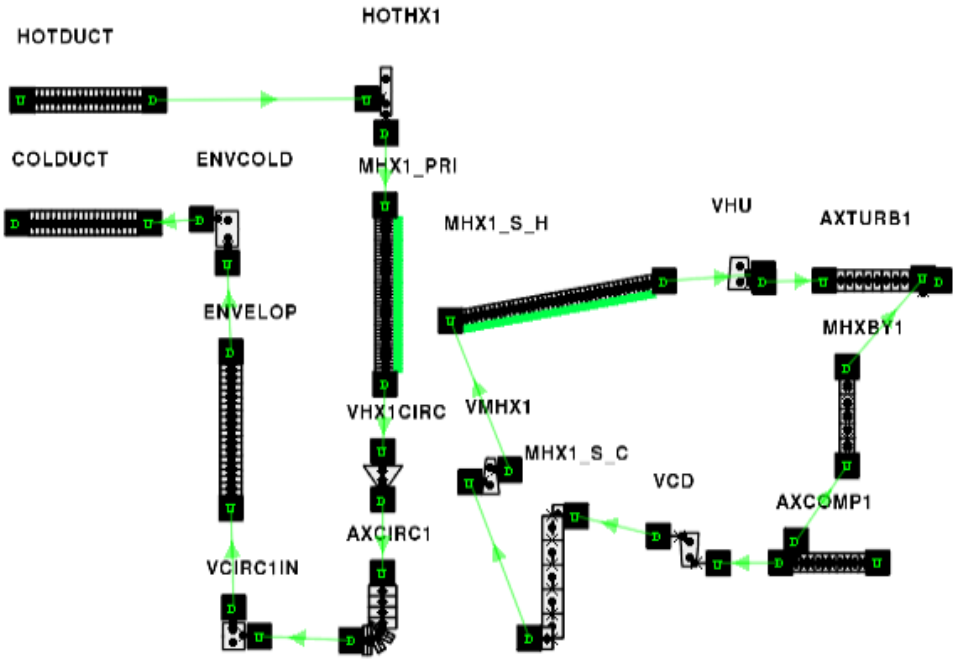

Figure EK_1: CATHARE nodalisation of the main heat exchanger

3.2 Secondary bypass

As shown in Figure EK_1, a bypass has been introduced to the secondary circuit as part of a further research regarding the model. It connects the outlet of the compressor with the outlet of the turbine and there are valves separating it from the regular flow. The bypass branch could be used to control the secondary flow through the heat exchanger. During the calculations EK made, the bypass valves have always been closed.

3.3 Material properties

The replacement of the secondary fluid requires the modification of the material properties. These properties are the following:

- specific heat capacity [J/kgK]
- specific gas constant [J/kgK]
- adiabatic exponent [-]

The helium-nitrogen gas mixture's properties have been calculated using its composition in mass ratio. In order to acquire the mass ratio of the components, it is necessary to know their molar mass and the ratio of their molar mass. The molar mass of nitrogen is 28 g/mol since it is a diatomic gas, while the molar mass of helium is 4,0026 g/mol. Knowing the ratio of their molar mass, the ratio of their mass can be calculated, as shown in Eq. EK_1.

$$\frac{m_N}{m_{He}} = \frac{n_N}{n_{He}} \cdot \frac{M_N}{M_{He}} \qquad \text{(EK\_1)}$$

Knowing the components' mass ratio to each other, the composition can be easily defined in mass ratio as well, which turns out to be 98,44% nitrogen and 1,56% helium.

To calculate the mixture's properties, the components' properties have been multiplied by their mass ratio and then added up. The material properties of each component and the mixture can be found in Table EK_2.

Table EK_2 Material properties for the secondary fluid

Material	Specific heat capacity [J/kgK]	Specific gas constant [J/kgK]	Adiabatic exponent [-]
Helium	5193	2077,22	1,66
Nitrogen	1040	593,4	1,404
Mixture	1104,79	616,754	1,408

3.4 Heat transfer correlation

In previous models, the Nusselt number and the heat transfer coefficient on the primary side of the main heat exchanger have been calculated using a built-in correlation, which CATHARE developers thought was the most suitable. However, in the case of such a complex geometry - like the helical tube bundle in a shell – finding the Nusselt number might require a more prudent approach. That is why both UJV and EK have tested six different correlations. The tested correlations – taken from [3] - are the following:

$$Nu_{v1} = 0{,}271 \cdot (f_a \cdot Re)^{0{,}624} \cdot Pr^{1/3} \quad \text{(EK\_2)}$$

$$Nu_{v2} = 0{,}0917 \cdot (f_a \cdot Re)^{0{,}725} \cdot Pr^{1/3} \quad \text{(EK\_3)}$$

$$Nu_{v3} = 0{,}16 \cdot (f_a \cdot Re)^{0{,}682} \cdot Pr^{1/3} \quad \text{(EK\_4)}$$

$$Nu_{v4} = 0{,}1135 \cdot (f_a \cdot Re)^{0{,}714} \cdot Pr^{1/3} \quad \text{(EK\_5)}$$

$$Nu_{v5} = 0{,}238 \cdot (f_a \cdot Re)^{0{,}634} \cdot Pr^{1/3} \quad \text{(EK\_6)}$$

$$Nu_{v6} = 0{,}1286 \cdot (f_a \cdot Re)^{0{,}692} \cdot Pr^{1/3} \quad \text{(EK\_7)}$$

Where f_a is the flow factor which is responsible for taking into account the geometry:

$$f_a = \frac{x_T - 1}{x_T \cdot \sqrt{1 + (x_L^2/16x_T^2) - 1}}. \quad \text{(EK\_8)}$$

In the term formula above x_T and x_L are the transversal and the longitudinal tube pitches, respectively.

3.5 Model summary

After several modifications described above, some of the CATHARE inputs at EK's disposal have been collected into Table EK_3, to better understand the differences between models. The highlighted input decks are referred to as *"Base model"* and "*New model"*.

Table EK_3 Some of EK's CATHARE input decks

Core power [MW]	Core type	Core inlet temp. [°C]	Core outlet temp. [°C]	Secondary fluid
75	MOX	260	520	water
75	MOXV2	260	520	water
75	REFRACTORY	260	520	water
75	REFRACTORY	400	800	water
75	**REFRACTORY**	**400**	**800**	**helium**
75	**REFRACTORY**	**400**	**800**	**nitrogen and helium**

4 CALCULATIONS

The main goal of the calculations done by EK was to provide system-code results for the new main heat exchanger design, both in the case of steady-state or transients. The different heat transfer correlations could also be tested under the same circumstances, providing a solid comparison base.

4.1 Steady State

4.1.1 Target values

Higher temperature and pressure values must be achieved in the secondary circuit to generate electricity efficiently. This means that different target values had to be set for the controls during the steady-state calculations.

The coolant flow was set to be 18,05 kg/s per loop on the primary side. This value differs from the one UJV used for their calculations because EK decided to stick with the 400°C coolant temperature increase on the core. The pressure at the inlet of the main heat exchanger on the primary side was set to be 6,94 MPa. The goal regarding the temperatures was to reach 400°C at the outlet of the main heat exchanger on the primary side, which means 800°C at the inlet, due to EK's decision to stick to the 400°C temperature difference. Achieving these numbers required some modifications, discussed in a later paragraph.

On the secondary side, the coolant flow's target value was 55,381 kg/s per loop, much higher than the 19,45 kg/s flow in the "base" models. The pressure at the inlet of the main heat exchanger on the secondary side was set to 22.5 MPa. The target value for the secondary coolant's temperature at the inlet of the MHX was 180°C, which could be easily set by changing the flow in the tertiary circuit.

4.1.2 Results regarding the different heat transfer correlations

One of EK's goals with the contribution was to test and compare the different heat transfer correlations, as it is written at the beginning of this chapter. The comparison was made by doing a steady-state calculation using each correlation, but all other parameters remained the same.

The mass flow rate was kept constant in the primary and secondary circuits of each simulation. Pressure drop coefficients control these flows, and the steady state cannot be considered good until these values are stable. The same applies to the secondary coolant's temperature at the inlet, precisely 180°C in each calculation.

The comparison is based on the temperatures on the primary side of the heat exchanger. The results are summarised in Table EK_4.

Table EK_4 MHX inlet and outlet temperatures on the primary side

Used correlation	Coolant temperature at the MHX primary inlet [°C]	Coolant temperature at the MHX primary outlet [°C]
v1	883,55	485,94
v2	898,7	501,16
v3	883,65	486
v4	888,2	490,5
v5	887,1	490
v6	894,9	497,4

There is a difference between the results for each correlation. Between the highest and the lowest inlet temperatures, there is a 15,15°C difference. Between the highest and lowest outlet temperatures, there is a 15,22°C difference. The correlation v2 produced the highest, and correlation v1 produced the lowest temperatures.

The evolution of the Nusselt number as a function of the Reynolds number (Figure EK_2) supports the results described above. The lowest Nusselt number comes from correlation v2, and the lowest Nusselt number results in the highest temperatures. There is a small difference between the correlations, resulting in the highest Nusselt number, which is projected onto the temperatures, but clearly, the best heat transfer comes from correlation v1 or v3.

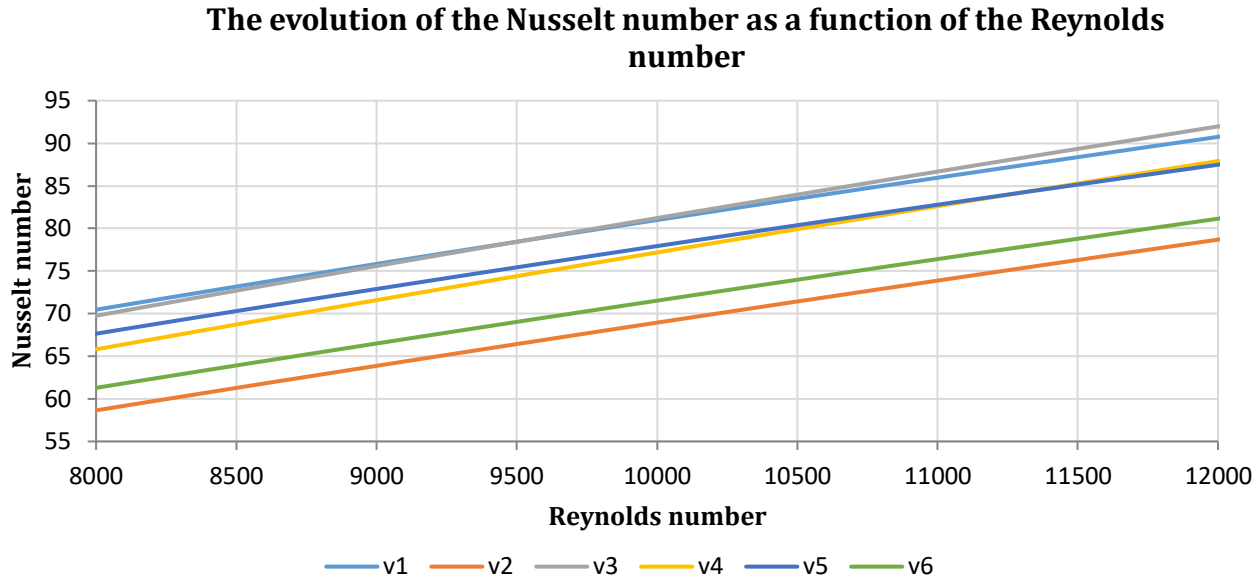

Figure EK_2: The evolution of the Nusselt number in the typical Reynolds number range

Correlation v2 was chosen to proceed with to remain conservative during further calculations.

4.1.3 Results regarding the target values

Primary coolant temperatures:

Apart from providing a great base for comparison, the results in Table EK_4 show another problem that had to be dealt with. The problem was that the temperature values were far from their target values. The inlet temperature had to be 800°C instead of around 900°C, and the outlet temperature had to be 400°C instead of about 500°C. This is the problem that has been referred to in paragraph 4.1.1.

The heat exchange surface had to be increased to bring the core inlet temperatures down by about 100°C. A bigger heat exchange surface means better heat exchange, resulting in lower temperatures. The easiest way to increase said surface is to increase the number of tubes in the heat exchanger. The number of tubes resulting in the correct temperatures has been determined during an iterative process. The effect of increasing the number of tubes had to be considered on the primary and secondary flow areas. Some steps of iteration are shown in Table EK_5.

Table EK_5 Steps of iteration to reach the correct primary temperatures

Number of heat exchange tubes	Coolant temperature at the outlet of the MHX [°C]
344	501,1
370	483,3
450	443,4
530	418
570	408,7
620	402

The number of heat exchange tubes had to be almost doubled to reach the target values, which resulted in the decrease of the primary flow area to 0,0987 m^2 from 0,598 m^2 and the increase of the secondary flow area to 0,1247 m^2 from 0,069 m^2. The geometry of the main heat exchanger remained the same

apart from the number of tubes. It is important to emphasize that these calculations used only the most conservative heat transfer correlation.

Secondary coolant temperatures:

On the secondary side, the increasing heat exchange surface has not significantly affected the temperatures. With the MHX inlet temperature strictly set to 180°C and the secondary mass flow rate being 55,381 kg/s, there is an 8°C difference in the secondary outlet temperature between the calculations using 344 and 620 tubes. The latter is higher, being 767,8°C.

4.2 Transient Calculations

As mentioned, the main goal was to provide steady-state and transient results with the new main heat exchanger design and the elevated secondary parameters. The chosen steady-state for the transient calculations was the one before any changes to the number of tubes and the one using the most conservative – v2 – Nusselt number correlation. Some of the most important values from the CATHARE calculations in steady state are presented below:

Primary circuit:

- core power: 75 MW
- primary mass flow rate: 18,05 kg/s
- core inlet temperature: 502,9°C
- core outlet temperature: 902,9°C
- core inlet pressure: 69,96 bar
- pressure drop on the core: 0,52 bar

Secondary circuit:

- MHX power: 37,5 MW
- secondary mass flow rate: 55,38 kg/s
- MHX inlet temperature: 180°C
- MHX outlet temperature: 759,5°C
- MHX inlet pressure: 225 bar

Tertiary circuit:

- tertiary mass flow rate: 870,35 kg/s
- aero inlet temperature: 25°C
- aero outlet temperature: 70,34°C

It must be mentioned that the turbines are probably not working correctly during both steady state and transient. That is because of the different secondary fluids. The turbines, which EK has access to, are optimised for pure helium, whose properties are far from the nitrogen–helium mixture. Hence, the turbines increase the temperature of the gas mixture by about 1.5 °C in a steady state. The excess heat is removed by a larger tertiary flow to compensate for the irregular behaviour of the turbines. Nevertheless, the MHX is the focus of this study, and the turbocompressors serve as a boundary condition for the CATHARE calculations. Further input deck improvement will be possible when the turbine and compressor are designed and their maps are available.

4.2.1 The selected transients

At the beginning of the SafeG project, a detailed transient analysis was conducted to find the most limiting transients for the ALLEGRO core optimisation. This work selected four initiating events, two

from the protected and two from the unprotected cases. Remaining on this basis, we selected three out of the four.

4.2.2 TR15

TR15 is a loss of flow accident (LOFA), where there is a 100% hot duct break in LOOP1, aggravated by an accidental DHR valve opening. Scram is available for this transient, and it is activated 0,01 s after the calculation starts due to the Power/Flow ratio rising to 130% of the nominal value. Although there is a 2 s delay in the actuation of the scram mechanism, the total power falls below 10% of the nominal at 2.5 s.

Temperature limits:

The peak cladding and fuel temperatures are the most important values to be checked. TR15 is a Category 4 accident, meaning the limit for the peak cladding temperature is 1600°C [4].

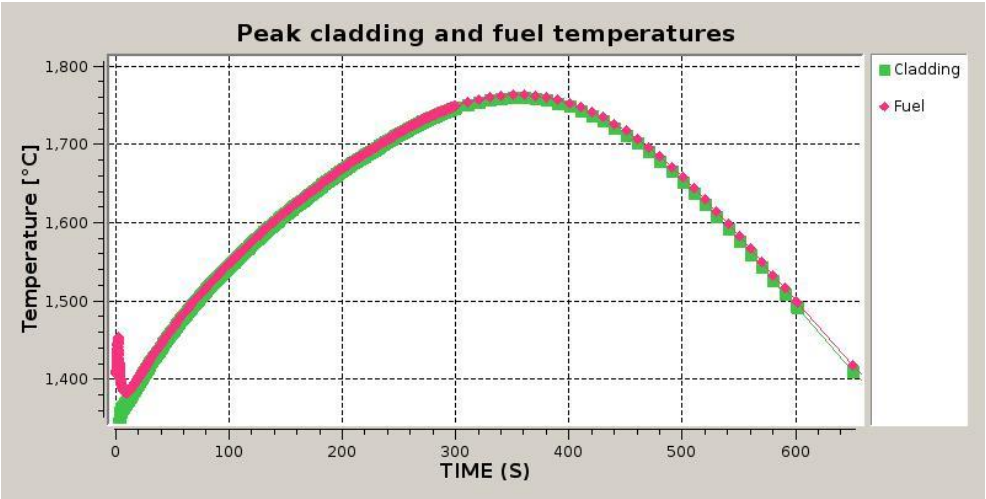

Figure EK_3: TR15 - Peak cladding and fuel temperatures

As seen in Figure EK_3, the peak cladding and peak fuel temperatures are almost the same. That is because of the scram, which radially equalises the temperatures across the fuel. The exact values are 1760°C for the PCT and 1763°C for the PFT. The PFT is far from the carbide fuel's melting point, about 2200°C [??ref??], but the PCT exceeds its limit by 160°C. The PCT is reached at 350 s.

MHX primary side:

This section investigates the MHX's behaviour during transients, so some main temperature and mass flow rate values must be shown.

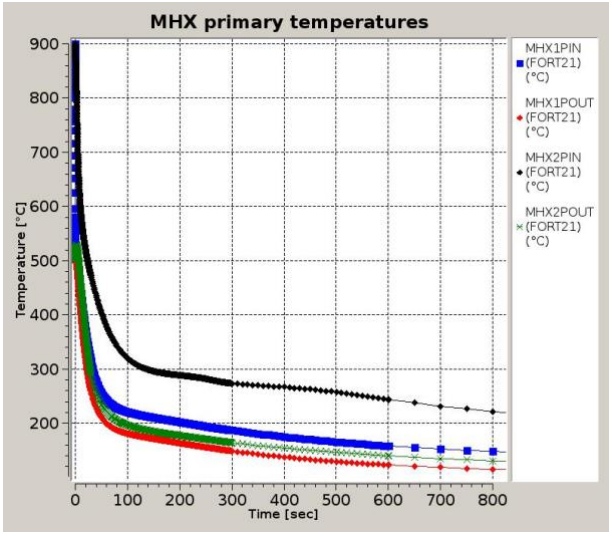

Figure EK_4: TR15 - Temperatures on the primary side of the MHX

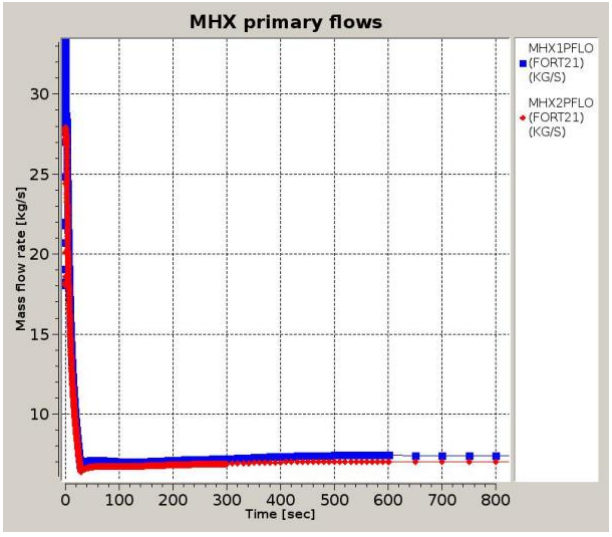

Figure EK_5: TR15 - Mass flow rates on the primary side of the MHX

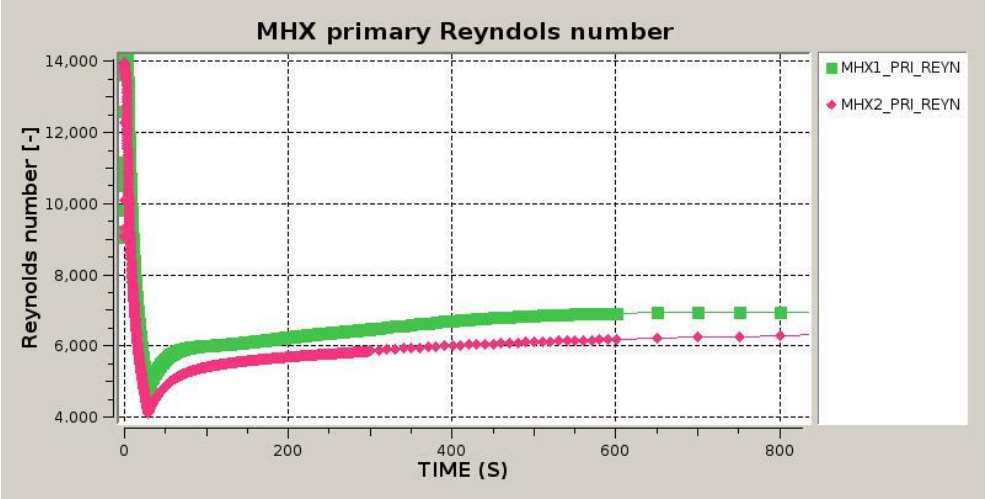

Figure EK_6: TR15 - Reynolds number on the primary side of the MHX

In Figures EK_4 to EK_6, both main heat exchangers are presented as marked in the values' names with either 1 for LOOP1 or 2 for LOOP2. The temperature decrease follows the power decrease due to the scram, while the temperature difference also decreases on the main heat exchanger despite the lower mass flow rate. The mass flow rate decreases because the open DHR loop partially bypasses the main loop.

The temperature and mass flow rate evolution in MHX differs for the two main loops. Since the break in the first loop has to deal with a lower pressure difference, its blower produces a higher mass flow rate in the first MXH primary side (its coolant bypasses the flow). This causes a difference in the Reynolds numbers, which is higher in LOOP1. A lower Reynolds number means worse heat exchange as seen in Figure EK_6, which generally results in higher temperatures. The ΔT is also different for the two loops, thanks to the slightly different mass flow rates.

The applicability of the Nusselt number correlation shown in Eq.EK_3 is not violated because we are still in the turbulent flow domain.

<u>MHX secondary side:</u>

Examining the main heat exchanger's secondary side requires attention, too.

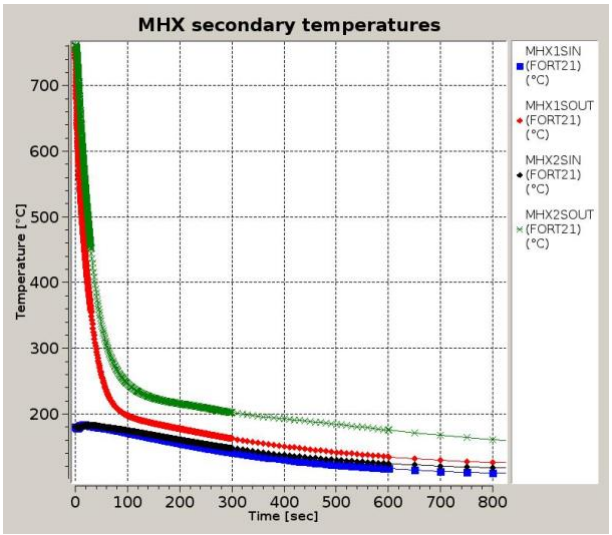

Figure EK_7: TR15 - Temperatures on the secondary side of the MHX

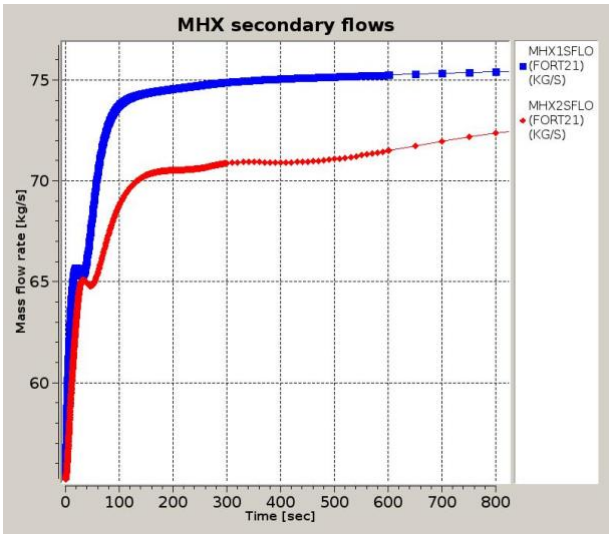

Figure EK_8: TR15 - Mass flow rates on the secondary side of the MHX

The secondary temperatures also follow the power decrease with the shrinking temperature differences. The secondary mass flow rates are rising due to the fixed rotational speed of the compressor, which is synchronised to the grid.

Conclusion:

TR15 does not satisfy the corresponding PCT criterion at the current model status. Nevertheless, we call the reader's attention to the fact that the current turbomachinery is optimised for the COUPLED ALLERGO CEA model, which contains pure helium coolant on the secondary side.

4.2.3 TR16

TR16 is a loss of coolant accident (LOCA), with a 10-inch break on the cold duct in LOOP1. It is aggravated by the same inadvertent DHR valve opening as in TR15. Scram is also commenced for this transient, and the signal is activated at 0,01 s because the Power/Flow rate ratio has increased by 30%. Although there is a 2 s delay in the actuation of the scram mechanism, the total power falls below 10% of the nominal at 2.5 s.

Temperature limits:

TR16 is a Category 4 initiating event, so the PCT limit is 1600°C. PCT and PFT evolutions are shown in Figure EK_9.

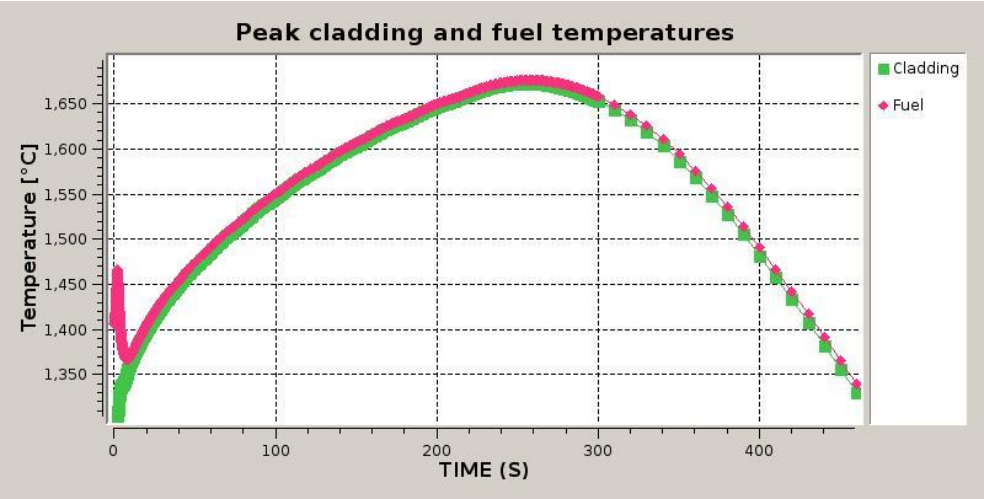

Figure EK_9: TR16 - Peak cladding and fuel temperatures

In this case, scram is equalising the cladding end fuel temperatures, too, and neither reaches 1700°C. The exact value for the PCT is 1673°C, reached at 255 s, while the PFT is 1676°C at 258 s. PFT does not exceed its limit again, but PCT is over 1600°C with 70°C.

MHX primary side:

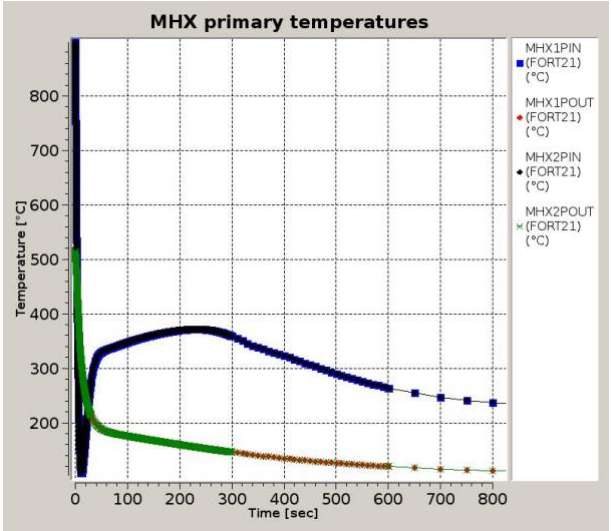

Figure EK_10: TR16 - Temperatures on the primary side of the MHX

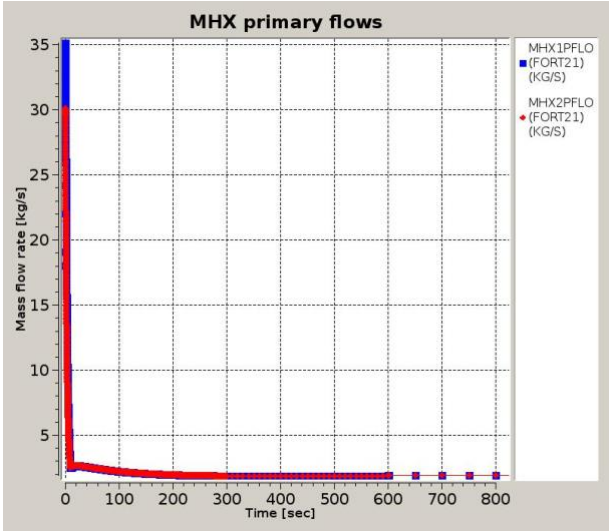

Figure EK_11: TR16 - Mass flow rates on the primary side of the MHX

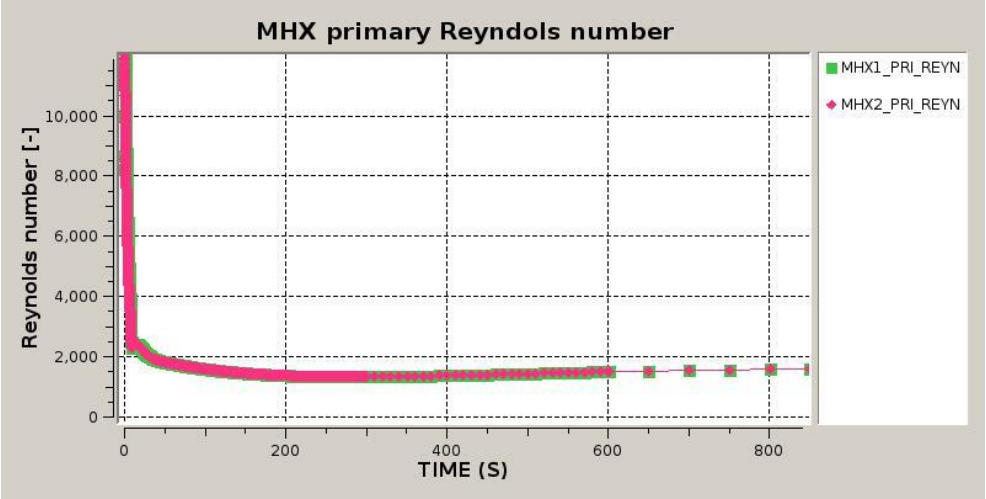

Figure EK_12: TR16 - Reynolds number on the primary side of the MHX

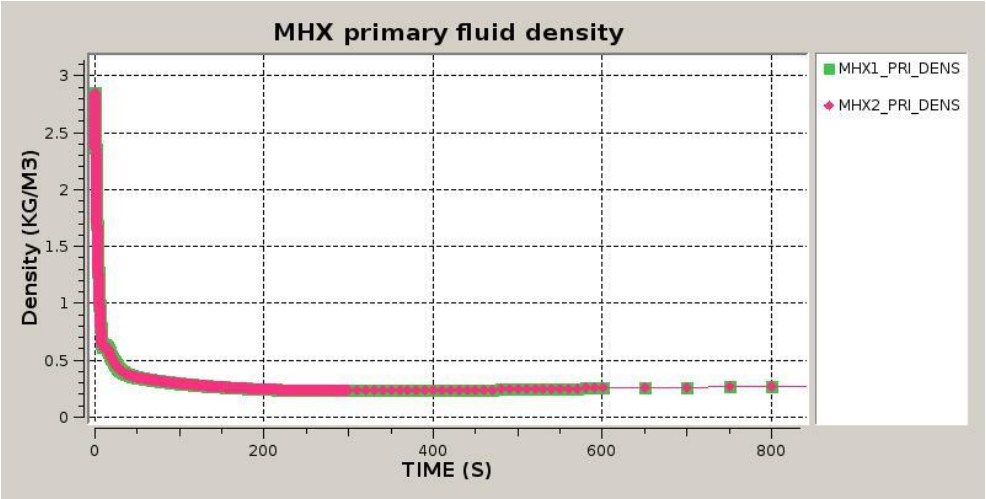

Figure EK_13: TR16 – Coolant density on the primary side of the MHX

The notations follow the same principle as in the case of TR15. During loss of coolant accidents, the primary fluid quickly cools down, resulting in the temperature drop seen in Figure EK_10. The decreasing power also causes the coolant temperatures to drop. The combination of these effects results in a short period (~30s) when both fluids are warming up the main heat exchanger. The heat stored in the main heat exchanger's walls provides the required heat. The primary inlet temperature increases back to be higher than the outlet temperature as the primary flow stabilises.

The pony motors drive the main blowers at 100 % speed of the nominal value. Because of the lower density, caused by the break, the mass flow rate decreases significantly and stabilises at around 2 kg/s. The low stabilised mass flow rate is aggravated by the accidentally opened DHR loop – causing a core bypass.

Due to the loss of coolant from the primary circuit, the density drops significantly. The stabilised value is 10% of the nominal. The significant decrease in the density and mass flow rate causes the Reynolds number to decrease, which results in worse heat exchange. Still, more importantly, it endangers the applicability of the used Nusselt number correlation, as we are on the verge of the laminar flow domain.

MHX secondary side:

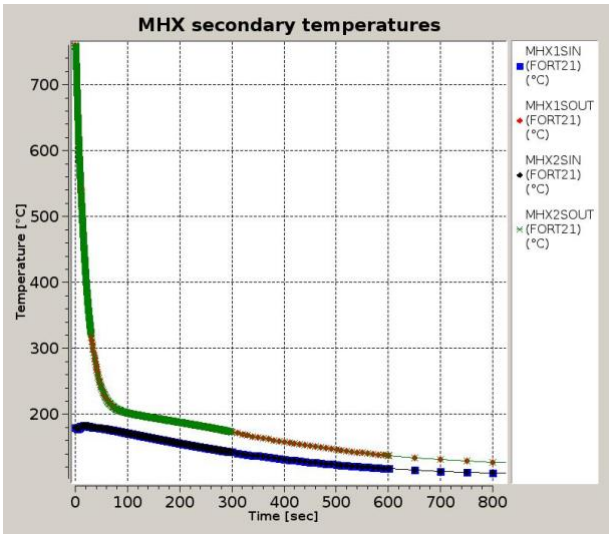

Figure EK_14: TR16 - Temperatures on the secondary side of the MHX

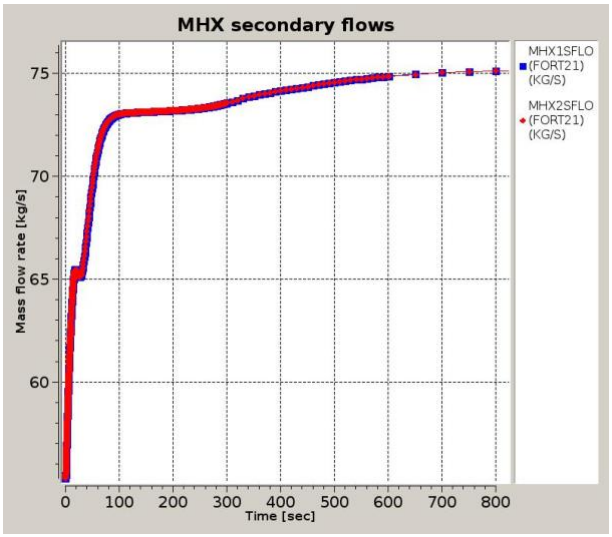

Figure EK_15: TR16 - Mass flow rates on the secondary side of the MHX

The secondary flow evolutions are mainly controlled by the turbocompressor and turbine, which are coupled to the electrical grid and have a constant rotational speed in this transient. Since the density decreases in the secondary loop, the mass flow rate increases at the constant compressor speed, see Figure EK_15.

Conclusion:

TR16 does not satisfy the corresponding PCT criterion at the current model status, but the effect of revised turbo machinery should be investigated. Since the results showed the Reynolds numbers falling in the range of the laminar region, the model's validity needs to be checked further.

4.2.4 TR20

TR20 is an unprotected loss of coolant accident with a break size of 3 inches. In the absence of scram, the reactivity feedback plays a decisive role in the transient evolution. In this transient, the main blowers rotate at 100% of their rotational speed. The nitrogen injection is activated at 56 s, when the primary pressure drops below 15 bar.

Temperature limits:

TR20 is a DEC A event, which means that the PCT limit is the carbide cladding's melting point, 2500°C. PCT and PFT evolutions are shown in Figure EK_16.

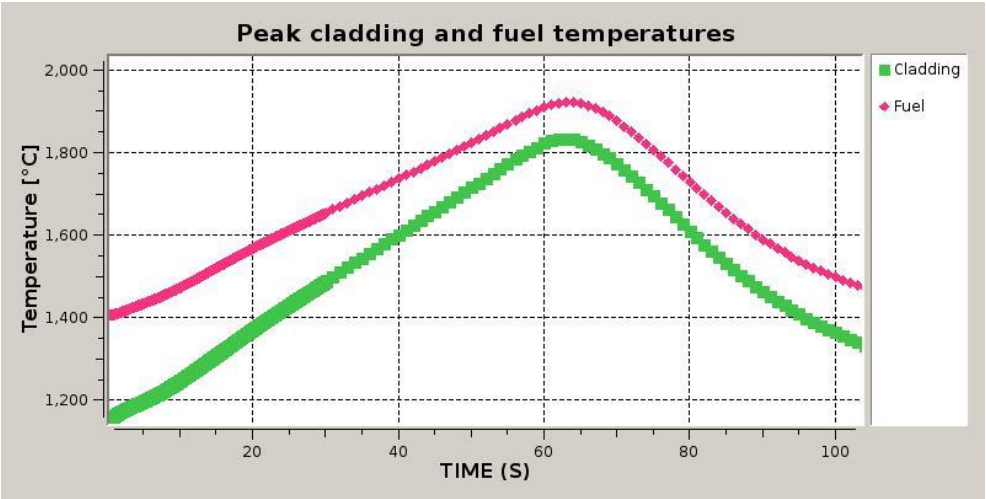

Figure EK_16: TR20 - Peak cladding and fuel temperatures

Without scram, the temperatures do not equalise radially in the fuel, so there is a visible difference between PCT and PFT. The PCT is 1834°C at 63 s, while the PFT is 1921°C reached at 64 s. With the PCT limit being 2500°C, TR20 is well below it.

MHX primary side:

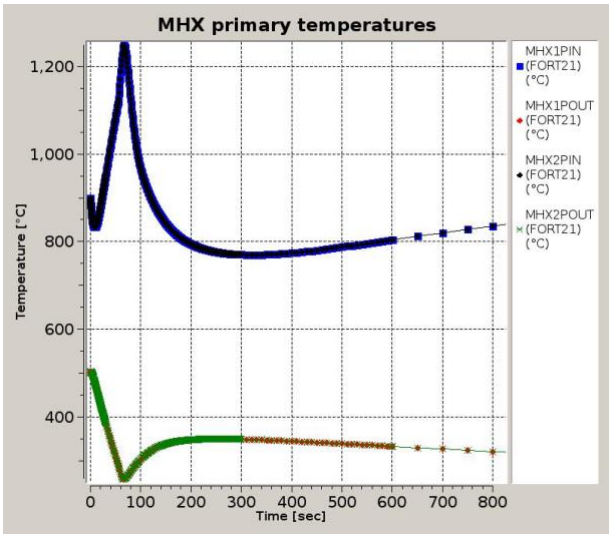

Figure EK_17: TR20 - Temperatures on the primary side of the MHX

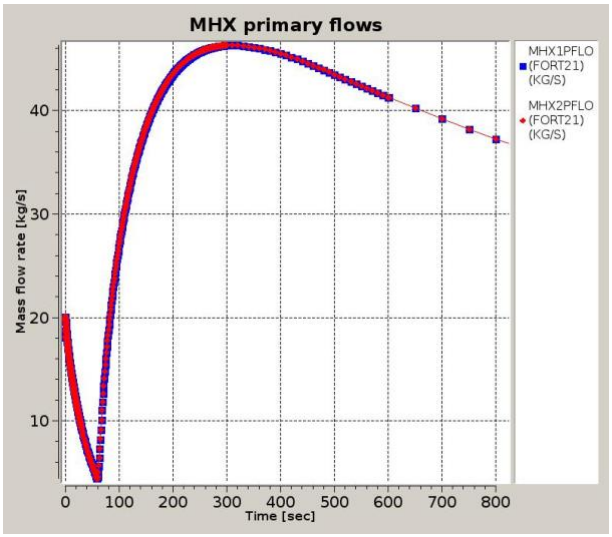

Figure EK_18: TR20 - Mass flow rates on the primary side of the MHX

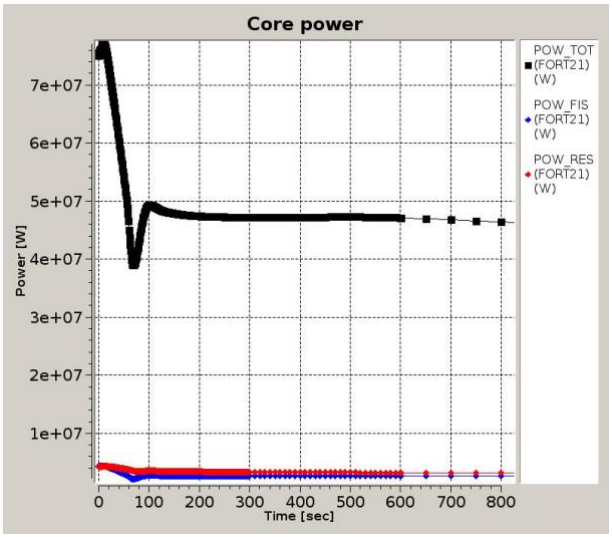

Figure EK_19: TR20 – Core power

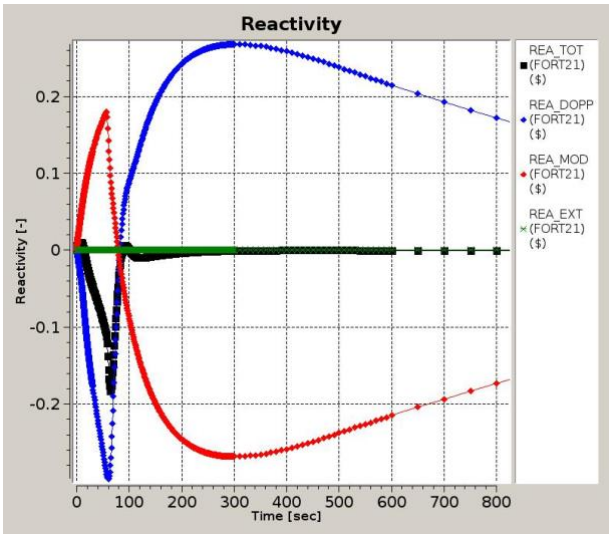

Figure EK_20: TR20 – Reactivity feedbacks

At the beginning of the transient, there is a small drop in the inlet temperature of the main heat exchangers, but the rapidly decreasing mass flow rates turn them around, and the inlet temperatures start to rise. At the same time, the core power starts to decrease because of the negative total reactivity, but with plummeting mass flow rates, the temperature differences on the main heat exchangers are rising.

At ~56 s, the lower plenum pressure falls below 15 bar, which triggers one of the nitrogen injection signals (lower plenum pressure<15 bar and no scram). The nitrogen injection immediately starts to drastically increase the mass flow rates in the main heat exchangers, which results in the decrease of the temperature differences on the main heat exchangers and the decrease of the temperatures themselves.

The higher mass flow rates result in lower temperatures in the core, too, which leads to positive Doppler reactivity feedback. The balance is restored by the reactivity feedback depending on the density of the primary coolant. As the density rises again due to the nitrogen injection, it balances out the positive Doppler feedback.

MHX secondary side:

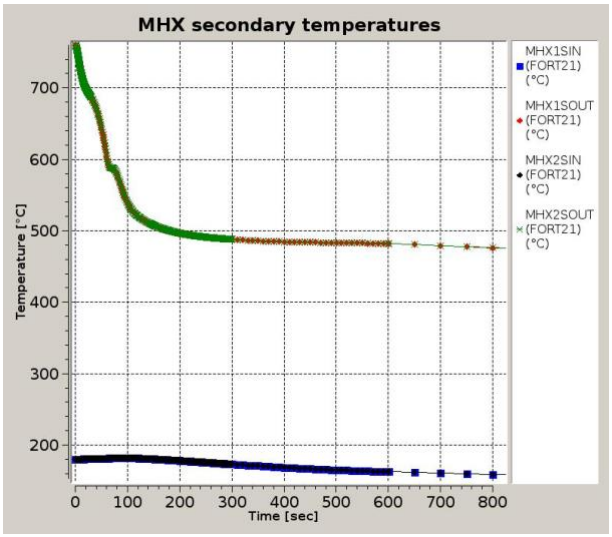

Figure EK_21: TR20 - Temperatures on the secondary side of the MHX

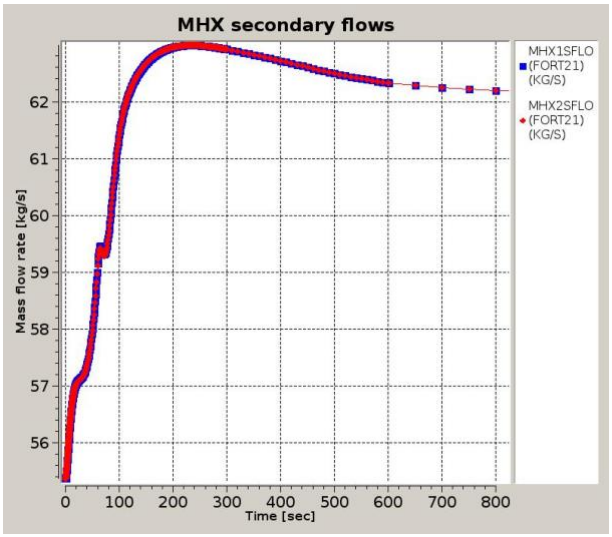

Figure EK_22: TR20 - Mass flow rates on the secondary side of the MHX

With the core power stabilising at about 60% of the nominal value, the temperature differences do not shrink as much as during protected transients.

The secondary mass flow rate increases because the coolant density decreases, and the turbomachinery speed is constant during the transient

Conclusion:

With the current nitrogen injection signal, TR20 fulfils the PCT criterion, but this transient also shows that the secondary circuits' behaviour requires further investigation. With the smaller break size, the nitrogen injection and the fully operational main blowers, the applicability of the Nusselt number correlation is not endangered.

4.2.5 TR22

TR22 is a rod group withdrawal transient, where 1$ of reactivity is introduced over 20 s. The transient is aggravated by an unavailable scram (UTOP).

At the beginning of the transient, the secondary pressure rises, and after 25 s, it reaches the limit of CATHARE, which is 260 bar.

Conclusion:

With the model's current state, TR22 cannot be examined thoroughly. Revising the turbomachinery in the secondary circuit would, without a doubt, allow us to investigate this transient more in detail.

5 CONCLUSIONS

This chapter investigates a new preconceptual main gas-gas heat exchanger (MHX) device designed by UJV. For the calculations, we used the CATAHRE thermal hydraulics system code. In this work, we developed a new CATHARE ALLEGRO input deck model which uses helium coolant on its secondary side. This model reached a new steady state with an elevated core outlet temperature of 800C.

It has to be emphasised that this current investigation focuses solely on the MHX performance in ALLEGRO and does not deal with the turbomachinery on the secondary side. On the other hand, we had to make some assumptions for the secondary compressor and turbine. Since the turbomachinery is not yet designed, we used the ALLEGRO COUPLED CEA model as a reference in this study. In that COUPLED model, the secondary coolant was pure helium, contrary to our model, which contains nitrogen and helium mixtures. Further, highlighting the differences, the CEA model was optimised for 65-70 bar pressure, instead of the UJV's 225 bar proposal. These are significant differences, and the turbomachinery here has to be considered a simple model, which gives boundary conditions for the calculations rather than an exact representation of the gas secondary circuit of a future ALLEGRO.

Based on our earlier IE selection work in SafeG [5], we selected four initiating events for this MHX investigation.

Using our current simplified CATHARE model, TR15 (100% hot duct break) does not satisfy the corresponding PCT criterion with the selected model parameters. Nevertheless, we call the reader's attention to the fact that the current turbomachinery is optimised for the COUPLED ALLERGO CEA model, which contains pure helium coolant on the secondary side at a significantly lower pressure than in the UJV's proposal.

The investigation of TR16 showed that the corresponding PCT is above the defined limit by 70°C, indicating the need for further optimisation of the secondary circuit because of the above mentioned issue. Since the results showed the Reynolds numbers falling in the range of the laminar region, the model's validity needs to be checked further.

With the current nitrogen injection signal, TR20 fulfils the PCT criterion, but this transient also shows that the secondary circuits' behaviour requires further investigation. With the smaller break size, the nitrogen injection and the fully operational main blowers, the applicability of the Nusselt number correlation is not endangered.

With the model's current state, TR22 cannot be examined thoroughly. Revising the turbomachinery in the secondary circuit would, without a doubt, allow us to investigate this transient more in detail.

In conclusion, the newly tested MHX design might cool the new refractory ALLEGRO core in steady-state conditions and some transients. However, new turbine and compressor maps are needed for a comprehensive safety analysis optimised for the new MHX design. The validity of the heat exchange correlations also has to be taken with care.

6 REFERENCES

[1] Y. Zheng, L. Shi, and Y. Wang, „Water-ingress analysis for the 200mwe pebble-bed modular high temperature gas-cooled reactor," *Nuclear Engineering and Design*, vol. 240, no. 10, pp. 3095–3107, 2010, 4th International Topical Meeting on High Temperature Reactor Technology (HTR 2008), with Regular Papers. [Online]. Available: https://www.sciencedirect.com/science/article/pii/S0029549310003547

[2] N. Tauveron and F. Bentivoglio, „Preliminary design and study of the indirect coupled cycle: An innovative option for gas fast reactor," *Nuclear Engineering and Design*, vol. 247, pp. 76–87, 2012. [Online]. Available: https://www.sciencedirect.com/science/article/pii/S0029549312000441

[3] M. Esch, A. Hurtado, D. Knoche, and W. Tietsch, „Analysis of the influence of different heat transfer correlations for htr helical coil tube bundle steam generators with the system code trace," *Nuclear Engineering and Design*, vol. 251, pp. 374–380, 2012, 5th International Topical Meeting on High Temperature Reactor Technology (HTR 2010). [Online]. Available: https://www.sciencedirect.com/science/article/pii/S002954931100851X

[4] Bálint Batki, Szabolcs Czifrus, Jan Klouzal, Sebastian Nyvlt, István Pataki, Petra Pónya, Annick Tosello, Petr Vacha, SAFEG D1.2 - Refractory core design, preparatory phase

[5] G. Mayer et al. SELECTION OF THE ENVELOPING TRANSIENTS OF ALLEGRO REACTOR AT THE BEGINNING OF THE SAFEG PROJECT, The 19th International Topical Meeting on Nuclear Reactor Thermal Hydraulics (NURETH-19) Log nr.: 35548 Brussels, Belgium, March 6 - 11, 2022